ELSEVIER

Chemical Engineering Journal 132 (2007) 241–255

Chemical Engineering Journal

www.elsevier.com/locate/cej

# Suction-lift sludge removal and non-Newtonian flow behaviour in circular secondary clarifiers: Numerical modelling and measurements

Michael Weiss [1], Benedek Gy. Plósz, Karim Essemiani *, Jens Meinhold

*Veolia Environnement Research & Development Center, Chemin de la Digue BP 76, 78603 Maisons-Laffitte Cedex, France*

Received 14 July 2006; received in revised form 29 December 2006; accepted 5 January 2007

**Abstract**

We present a computational fluid dynamics (CFD) model that predicts the sedimentation of activated sludge in a full-scale flat-bottom circular secondary clarifier that is equipped with a suction-lift sludge removal system. The axisymmetric single-phase model is developed using the general-purpose CFD solver Fluent. A convection–dispersion equation, which is extended to incorporate the sedimentation of activated sludge in the field of gravity, governs the mass transfer in the clarifier. Sludge removal by suction-lift in the near-bottom region of the clarifier is simulated using negative source terms on all field equations. The standard $k$–$\varepsilon$ turbulence model is used to compute the turbulent motion, and our CFD model accounts for buoyancy flow and non-Newtonian flow behaviour of the activated sludge in the clarifier. The rheological flow behaviour was measured for varying sludge concentrations and temperatures. These measurements show that at low to moderate shear rates typical of secondary clarifiers, the relationship between shear stress and shear rate follows the Casson law for pseudo-plastic flow behaviour. The rheology study was carried out together with measurements of the settling velocity during on-site measurements. The well-known double-exponential law is used to describe the dependence of the settling velocity on the concentration. Light scattering was applied to measure the local sludge distribution in the clarifier. The computation of the local sludge distribution in the clarifier by the CFD model compares well with concentration profile measurements for two different treatment plant loadings. Our CFD computations show further that the sludge viscosity dominates the flow and the sedimentation of activated sludge within the sludge blanket.


*Keywords:* Sedimentation; Secondary clarifier; Activated sludge; Rheology; Computational fluid dynamics; Suction-lift sludge removal

## 1. Introduction

Secondary clarifiers represent the final stage in the activated sludge wastewater treatment process (Fig. 1). They are preceded by the aeration basin, where previously developed biological sludge flocs are brought into contact with the organic material in the wastewater. Within the activated sludge process, secondary clarifiers fulfil a triple-role, acting as (i) clarifier, (ii) sludge thickener, and (iii) sludge storage zone. The clarifying function produces the clear supernatant, whereas the thickening function provides a continuous underflow of thickened sludge that is recycled to the aeration basin. The storage function ensures that sludge may be kept within the system during peak flows. Failure with respect to either of these functions can result in increased suspended solids concentrations in the effluent or in the deterioration of the entire activated sludge process. Practical experience has shown that the secondary clarifier is often the main bottleneck in the activated sludge process [1–4].

The present study concerns circular clarifiers that are equipped with suction-lift sludge removal systems. In these clarifier systems, which usually have a flat bottom, the sludge is withdrawn through an array of vertical suction (or aspiration) pipes from the near-bottom region (Fig. 2). These pipes are situated underneath the slowly rotating clarifier bridge and remove sludge locally underneath the bridge. This design form may be contrasted with clarifiers that have conical bottoms and bottom scraper systems, and where the sludge is removed centrally at the bottom through the sludge hopper. The latter design form has received considerable attention by researchers in recent years [5–7]. On the other hand, studies on clarifiers with flat (or nearly flat) bottoms that are equipped with suction-lift sludge removal systems are rare.

* Corresponding author. Tel.: +1 412 809 6112; fax: +1 412 809 6111.
*E-mail address:* karim.essemiani@veoliawater.com (K. Essemiani).
[1] Present address: Voith Paper Technology Center GmbH, Paul-Hartmann-Str. 4, 89522 Heidenheim, Germany.

1385-8947/$ – see front matter © 2007 Elsevier B.V. All rights reserved.
doi:10.1016/j.cej.2007.01.004

## Nomenclature

*Latin symbols*

| | |
|---|---|
| $C_1$ | constant in turbulence model |
| $A$ | parameter in sludge viscosity model ($m^{11/2}\,kg^{-3/2}\,s^{-1}$) |
| $C_2$ | constant in turbulence model |
| $B$ | parameter in sludge viscosity model ($m^{5/2}\,kg^{-1/2}\,s^{-1}$) |
| $C_3$ | constant in turbulence model |
| $C_\mu$ | constant in turbulence model |
| $D$ | clarifier diameter (m) |
| $f_{ns}$ | non-settleable fraction of solids in the effluent |
| $g$ | gravitational acceleration constant ($m\,s^{-2}$) |
| $G$ | generation of turbulence kinetic energy due to buoyancy ($kg\,m^{-1}\,s^{-3}$) |
| $h$ | height of sludge removal zone (m) |
| $H_{clarifier}$ | clarifier depth (m) |
| $H$ | height of sludge in the settling column (m) |
| $I_u$ | turbulence intensity |
| $k$ | turbulence kinetic energy ($m^2\,s^{-2}$) |
| $k_{in}$ | turbulence kinetic energy at the inlet ($m^2\,s^{-2}$) |
| $K_1$ | Casson yield stress parameter ($kg^{1/2}\,m^{-1/2}\,s^{-1}$) |
| $K_2$ | Casson viscosity parameter ($kg^{1/2}\,m^{-1/2}\,s^{-1/2}$) |
| $\bar{K}_2$ | mean Casson viscosity parameter ($kg^{1/2}\,m^{-1/2}\,s^{-1/2}$) |
| $L_u$ | turbulent length scale (m) |
| $p$ | pressure (Pa) |
| $P$ | generation of turbulence kinetic energy due to shear ($kg\,m^{-1}\,s^{-3}$) |
| $q_{rec}$ | recycle mass flow rate ($kg\,s^{-1}$) |
| $Q_{in}$ | flow rate at the clarifier inlet ($m^3\,s^{-1}$) |
| $r$ | radial coordinate (m) |
| $r_h$ | parameter describing hindered settling ($m^3\,kg^{-1}$) |
| $r_p$ | parameter describing particulate settling ($m^3\,kg^{-1}$) |
| $R_{a,i}$ | inner radius of the inlet annulus (m) |
| $R_{a,o}$ | outer radius of the inlet annulus (m) |
| $R_{baffle}$ | baffle skirt radius in the inlet region (m) |
| $R_i$ | inner radius of the sludge removal zone (m) |
| $R_o$ | outer radius of the sludge removal zone (m) |
| $S_k$ | sludge removal source term in equation for turbulent kinetic energy ($kg\,m^{-1}\,s^{-3}$) |
| $S_m$ | sludge removal source term in continuity equation ($kg\,m^{-3}\,s^{-1}$) |
| $S_r$ | sludge removal source term in radial momentum equation ($kg\,m^{-2}\,s^{-2}$) |
| $S_X$ | sludge removal source term in convection–dispersion equation ($kg^2\,m^{-6}\,s^{-1}$) |
| $S_z$ | sludge removal source term in axial momentum equation ($kg\,m^{-2}\,s^{-2}$) |
| $S_\varepsilon$ | sludge removal source term in equation for turbulent kinetic energy dissipation rate ($kg\,m^{-1}\,s^{-4}$) |
| $t$ | time (s) |
| $T$ | temperature (°C) |
| $u$ | axial velocity component ($m\,s^{-1}$) |
| $u_{in}$ | axial velocity component at the inlet ($m\,s^{-1}$) |
| $u_s$ | sludge settling velocity ($m\,s^{-1}$) |
| $u_{s0}$ | maximum sludge settling velocity ($m\,s^{-1}$) |
| $v$ | radial velocity component ($m\,s^{-1}$) |
| $v_{in}$ | radial velocity component at the inlet ($m\,s^{-1}$) |
| $V_{rec}$ | volume of the sludge removal zone ($m^3$) |
| $X$ | sludge concentration ($kg\,m^{-3}$) |
| $X_{in}$ | sludge concentration at the inlet ($kg\,m^{-3}$) |
| $X_{ns}$ | concentration of non-settleable sludge fraction ($kg\,m^{-3}$) |
| $X^*$ | sludge concentration at transition point ($kg\,m^{-3}$) |
| $z$ | axial coordinate (m) |

*Greek symbols*

| | |
|---|---|
| $\alpha$ | correlation parameter ($m\,h^{-1}$) |
| $\beta$ | correlation parameter ($g\,ml^{-1}$) |
| $\delta$ | correlation parameter ($l\,ml^{-1}$) |
| $\varepsilon$ | turbulent kinetic energy dissipation rate ($m^2\,s^{-3}$) |
| $\varepsilon_{in}$ | turbulent kinetic energy dissipation rate at the inlet ($m^2\,s^{-3}$) |
| $\gamma$ | correlation parameter ($l\,g^{-1}$) |
| $\dot{\gamma}$ | shear rate ($s^{-1}$) |
| $\kappa$ | von Kármán constant |
| $\mu$ | sludge viscosity ($kg\,m^{-1}\,s^{-1}$) |
| $\mu_t$ | turbulent viscosity ($kg\,m^{-1}\,s^{-1}$) |
| $\mu_w$ | viscosity of water ($kg\,m^{-1}\,s^{-1}$) |
| $\rho$ | sludge density ($kg\,m^{-3}$) |
| $\rho_p$ | dry sludge density ($kg\,m^{-3}$) |
| $\rho_w$ | density of water ($kg\,m^{-3}$) |
| $\sigma_k$ | turbulent Prandtl number for $k$ |
| $\sigma_s$ | turbulent Schmidt number |
| $\sigma_\varepsilon$ | turbulent Prandtl number for $\varepsilon$ |

Computational fluid dynamics (CFD), which resolves the fluid mechanics and the sludge transport locally in the clarifier, is often used for designing and optimising new and existing secondary clarifiers, and to detect the causes of malfunction of these process separation units. For example, short circuits in the clarifier, a local hydraulic phenomenon, can result in the dilution of the sludge in the recirculation stream to the aeration basin, so that the concentration in the aeration basin falls below the value necessary for the efficient conversion of the organic matter in the wastewater. A local hydraulic problem can thus lead to the deterioration of the entire activated sludge process.

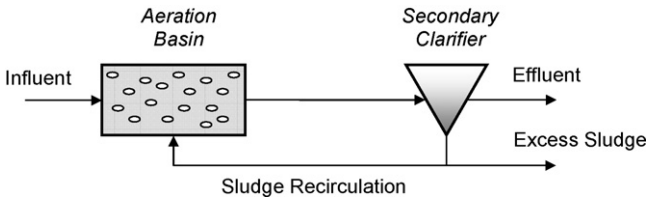


Fig. 1. Schematic representation of the activated sludge wastewater treatment process.

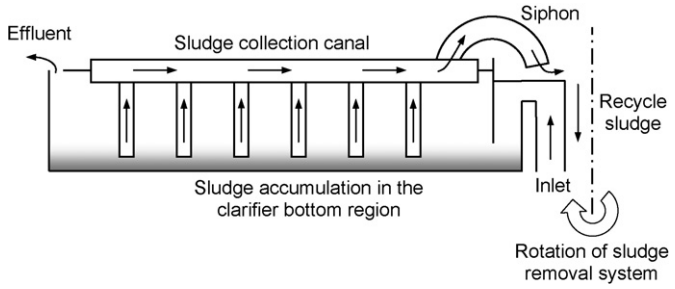


Fig. 2. Schematic drawing of the flat-bottom clarifier showing the inlet annulus and the effluent outlet. The dash-dotted line marks the vertical centre line of the axisymmetric clarifier basin. The slowly rotating array of vertical suction pipes withdraws settled sludge from the near-bottom region of the clarifier into the sludge collection canal. The thickened sludge passes through the siphon and is recycled to the aeration basin.

Other areas of application for CFD modelling techniques in the wastewater treatment process include sludge digestion, where the excess activated sludge that is withdrawn from the process (Fig. 1) is digested to produce methane. For example, Keshtkar et al. presented a mathematical model of an anaerobic digester for cattle manure, which includes a model for the microbial kinetics and that describes the non-ideal mixing behaviour in the continuous flow reactor [8]. Their computations show that deviations from the ideal mixing regime decrease the methane yield. Vesvikar and Al-Dahhan used a liquid/gas CFD model to analyse the flow pattern in an anaerobic digester [9]. The authors compared their computed data with flow visualisation experiments. The overall flow pattern, the location of circulation cells and regions of stagnant flow in the experiment and in the CFD prediction agreed well. They have used their CFD model to study the effects of changing draft tube sizes, clearance, and shape of the digester bottom on the flow pattern.

CFD modelling techniques are also used to study mixing and oxygen transfer in the aeration basin. To support start-up procedures and to verify equipment performance, Essemiani et al. simulated the velocity field in two types of aeration basins for clear water and without aeration [10]. The CFD prediction of the velocity field was shown to be in good agreement with local velocity measurements. Using a two-phase flow modelling technique, Glover et al. extended the CFD model of the aeration basin to account for the aeration phase [11]. Further, using scalar transport equations and conversion reaction mechanisms, they implemented the biological conversion of the organic matter in the wastewater. The comparison with measurements of the various components over time (ammonia, nitrate, and dissolved oxygen) showed excellent agreement with the CFD predictions. However, the CFD model under-predicts the chemical oxygen demand by about 30%. The authors attribute this difference to the addition of anti-foaming agent, which is not accounted for in the CFD model.

Our study describes a CFD model of the flat-bottom secondary clarifiers at a wastewater treatment plant in the north-west of France, which has been constructed for 122,000 inhabitant-equivalents and that consists of two identical biological treatment lines. Each treatment line consists of one continuously fed aeration basin and two identical secondary clarifiers.

The CFD model presented in this paper, which we have developed using the general-purpose CFD solver Fluent, rests on the numerical model presented by Lakehal et al. [5]. It differs from that of the aforementioned authors in mainly two ways: (i) it employs negative source terms on the governing field equations that represent the removal of settled sludge by suction-lift, and (ii) it uses the Casson rheology model instead of the Bingham rheology model to reflect the non-Newtonian flow behaviour of the activated sludge mixture in the clarifier.

We have carried out on-site measurements to determine the rheological flow behaviour of the sludge mixture. A detailed description of these measurements and our rheology analysis may be found elsewhere [12]. Measurements of the settling velocity of the sludge flocs were conducted in addition to our rheology studies. Furthermore, the boundary conditions for the CFD model, such as the inlet concentration and the flow rates, were determined. We have measured concentration profiles within the clarifier to validate the numerical model.

All measurements were conducted in March and April 2005, and again in July of the same year, which enabled us to study periods of low and high treatment plant loadings, respectively. The wastewater treatment plant, on which we conducted the study presented in this paper, is situated in a region of France that is frequented by a large number of tourists in the summer months, which explains the increase in treatment plant loading in July.

## 2. Mathematical model

### 2.1. Reynolds-averaged Navier–Stokes equations

The system of Reynolds-averaged Navier–Stokes equations for two-dimensional, axisymmetric, unsteady, density-stratified, and turbulent mean flow may be given as [3,5–7]

$$\rho_{\mathrm{w}}\left(\frac{\partial u}{\partial z}+\frac{\partial v}{\partial r}+\frac{v}{r}\right)=S_{\mathrm{m}}, \tag{1}$$

$$\begin{aligned}&\rho_{\mathrm{w}}\left(\frac{\partial u}{\partial t}+\frac{\partial u^2}{\partial z}+\frac{\partial(uv)}{\partial r}\right)\\&\quad=-\frac{\partial p}{\partial z}+\frac{\partial}{\partial z}\left(2(\mu+\mu_{\mathrm{t}})\frac{\partial u}{\partial z}\right)\\&\qquad+\frac{1}{r}\frac{\partial}{\partial r}\left(r(\mu+\mu_t)\left(\frac{\partial u}{\partial r}+\frac{\partial v}{\partial z}\right)\right)-g(\rho-\rho_{\mathrm{w}})+S_z,\end{aligned} \tag{2}$$

and

$$\begin{aligned}&\rho_{\mathrm{w}}\left(\frac{\partial v}{\partial t}+\frac{\partial(uv)}{\partial z}+\frac{\partial v^2}{\partial r}\right)\\&\quad=-\frac{\partial p}{\partial r}+\frac{\partial}{\partial z}\left((\mu+\mu_{\mathrm{t}})\left(\frac{\partial u}{\partial r}+\frac{\partial v}{\partial z}\right)\right)\\&\qquad+\frac{1}{r}\frac{\partial}{\partial r}\left(2r(\mu+\mu_t)\frac{\partial u}{\partial r}\right)-\frac{2(\mu+\mu_{\mathrm{t}})}{r}\frac{v}{r}+S_{\mathrm{r}}.\end{aligned} \tag{3}$$

The equation of continuity is given by Eq. (1), and Eqs. (2) and (3) represent the $z$ and $r$ momentum conservation equations, respectively. The origin of the coordinate system is placed on the vertical centre line, with the $z$-axis pointing vertically upwards from the bottom boundary. We note that the field equations are given in terms of averaged flow variables, where $u$ and $v$ are the mean velocity components in the $z$ (axial) and $r$ (radial) directions, respectively, $t$ is the time, $p$ is the pressure, $\rho$ is the density of the mixed liquor, $\rho_w$ is the density of water, $g$ is the gravitational acceleration constant, $\mu$ is the viscosity of the sludge mixture, and $\mu_t$ is the turbulent viscosity.

The governing field equations are formulated using the density of water, and we account for the varying density of the sludge mixture only in the buoyancy term in the axial momentum equation, $g(\rho - \rho_w)$. We add the buoyancy term to the $z$ momentum equation using a user-defined function (UDF) in Fluent.

The on-site density measurements of Dahl have shown that the relative density increase at a total suspended solids concentration of 12 kg m$^{-3}$ is only 0.4% [13]. However, the buoyancy effect on the flow in the clarifier that is caused by the density gradient at the upper limit of the sludge blanket cannot be neglected.

We have added source terms to Eqs. (1)–(3) that represent sludge removal by suction-lift. These source terms are defined as

$$S_m = -\frac{q_{rec}}{V_{rec}}, \tag{4}$$

$$S_z = -\frac{q_{rec}}{V_{rec}} u, \tag{5}$$

and

$$S_r = -\frac{q_{rec}}{V_{rec}} v, \tag{6}$$

and they are built into the CFD model using UDFs. The source terms are negative since sludge is removed from the system. In Eqs. (4)–(6), $q_{rec}$ is the mass flow rate of the recycle stream in kg s$^{-1}$, and $V_{rec}$ is the volume of the sludge removal zone in the near-bottom region of the clarifier in m$^3$. The recycle mass flow rate is obtained from flow measurements around the clarifier, and the volume of the sludge removal zone is defined further down in the paper. The source term $S_m$ represents the withdrawal of sludge mass from the bottom region of the clarifier. The source terms $S_z$ and $S_r$ account for the momentum change that is associated with the removal of sludge mass in the removal zone. All source terms are zero outside the sludge removal zone.

### 2.2. Standard $k$–$\varepsilon$ turbulence model

The turbulent (or eddy) viscosity, $\mu_t$, is determined by the turbulent kinetic energy, $k$, and also by the rate of dissipation of turbulence kinetic energy, $\varepsilon$, according to

$$\mu_t = \rho_w C_\mu \frac{k^2}{\varepsilon}, \tag{7}$$

where $C_\mu = 0.09$ is a constant. The semi-empirical model transport equations for $k$ and $\varepsilon$ may be given as [3,5–7]

$$\rho_w \left( \frac{\partial k}{\partial t} + \frac{\partial (uk)}{\partial z} + \frac{\partial (vk)}{\partial r} \right) = \frac{\partial}{\partial z} \left( \left( \mu + \frac{\mu_t}{\sigma_k} \right) \frac{\partial k}{\partial z} \right) + \frac{1}{r} \frac{\partial}{\partial y} \left( y \left( \mu + \frac{\mu_t}{\sigma_k} \right) \frac{\partial k}{\partial r} \right) + P + G - \rho_w \varepsilon + S_k, \tag{8}$$

and

$$\rho_w \left( \frac{\partial \varepsilon}{\partial t} + \frac{\partial (u\varepsilon)}{\partial z} + \frac{\partial (v\varepsilon)}{\partial r} \right) = \frac{\partial}{\partial z} \left( \left( \mu + \frac{\mu_t}{\sigma_\varepsilon} \right) \frac{\partial \varepsilon}{\partial z} \right) + \frac{1}{r} \frac{\partial}{\partial r} \left( r \left( \mu + \frac{\mu_t}{\sigma_\varepsilon} \right) \frac{\partial \varepsilon}{\partial r} \right) + C_1 \frac{\varepsilon}{k} (P + G - C_3 G) - \rho_w C_2 \frac{\varepsilon^2}{k} + S_\varepsilon, \tag{9}$$

respectively, where

$$P = \mu_t \left[ 2 \left( \frac{\partial u}{\partial r} \right)^2 + 2 \left( \frac{\partial v}{\partial z} \right)^2 + 2 \left( \frac{u}{r} \right)^2 + \left( \frac{\partial u}{\partial z} + \frac{\partial v}{\partial r} \right)^2 \right] \tag{10}$$

is the generation of turbulence kinetic energy due to mean velocity gradients, that is, due to shear, and

$$G = -g \frac{\mu_t}{\rho_w \sigma_t} \frac{\partial \rho}{\partial z} \tag{11}$$

corresponds to the generation of turbulence kinetic energy due to buoyancy. In Eq. (11), $\sigma_t = 0.85$ is the turbulent Prandtl number. Eq. (11) is implemented into the CFD model using a UDF.

In Eqs. (8) and (9), $\sigma_k = 1.0$ and $\sigma_\varepsilon = 1.3$ are the turbulent Prandtl numbers for $k$ and $\varepsilon$, respectively. In Eq. (9), $C_1 = 1.44$ and $C_2 = 1.92$ are constants. For stably stratified flow, which prevails in secondary clarifiers and which tends to suppress turbulence ($G < 0$), the constant $C_3$ takes a value of 0.8–1.0 [5]. Note that the gravity vector in our model is $-g$ as it points in the negative axial direction. Assuming $C_3 = 1.0$, Eq. (9) reduces to

$$\rho_w \left( \frac{\partial \varepsilon}{\partial t} + \frac{\partial (u\varepsilon)}{\partial z} + \frac{\partial (v\varepsilon)}{\partial r} \right) = \frac{\partial}{\partial z} \left( \left( \mu + \frac{\mu_t}{\sigma_\varepsilon} \right) \frac{\partial \varepsilon}{\partial z} \right) + \frac{1}{r} \frac{\partial}{\partial r} \left( r \left( \mu + \frac{\mu_t}{\sigma_\varepsilon} \right) \frac{\partial \varepsilon}{\partial r} \right) + C_1 \frac{\varepsilon}{k} P - \rho_w C_2 \frac{\varepsilon^2}{k} + S_\varepsilon, \tag{12}$$

so that the effect of buoyancy on the rate of dissipation of turbulence kinetic energy is not considered. Eqs. (8) and (12) are used in our CFD model to compute $k$ and $\varepsilon$.

Two source terms $S_k$ and $S_\varepsilon$ appear in Eqs. (8) and (12), respectively, which we use to take the effect of the sludge removal on the turbulence kinetic energy and its dissipation rate into account. Both $S_k$ and $S_\varepsilon$, which are defined as

$$S_k = -\frac{q_{rec}}{V_{rec}} k \tag{13}$$

and

$$S_\varepsilon = -\frac{q_{\mathrm{rec}}}{V_{\mathrm{rec}}}\varepsilon, \tag{14}$$

respectively, are built into the CFD model using UDFs.

### 2.3. Conservation of particulate mass in turbulent flows

The sludge transport equation for turbulent flow may be written as [5,6,14]

$$\rho_{\mathrm{w}}\left(\frac{\partial X}{\partial t} + \frac{\partial((u-u_{\mathrm{s}})X)}{\partial z} + \frac{\partial(vX)}{\partial r}\right) = \frac{\partial}{\partial z}\left(\frac{\mu_{\mathrm{t}}}{\sigma_{\mathrm{s}}}\frac{\partial X}{\partial z}\right) + \frac{1}{r}\frac{\partial}{\partial r}\left(r\frac{\mu_{\mathrm{t}}}{\sigma_{\mathrm{s}}}\frac{\partial X}{\partial r}\right) + S_X, \tag{15}$$

where $\sigma_{\mathrm{s}}$ is the turbulent Schmidt number, $u_{\mathrm{s}} = u_{\mathrm{s}}(X)$ is the settling velocity function, which we discuss further down in the paper, and $S_X$ is the sludge removal source term, given by

$$S_X = -\frac{q_{\mathrm{rec}}}{V_{\mathrm{rec}}}X. \tag{16}$$

In Eq. (15), the sedimentation of activated sludge is accounted for in the axial convection term. Other researchers have added the settling velocity function to the mass transport equation using a source term on the right-hand side of Eq. (15) [15,16]. Typical values for the turbulent Schmidt number are in the range 0.5–1.0 [3]. We use the value proposed by Lakehal et al., that is, $\sigma_{\mathrm{s}} = 0.7$ [5].

We have added Eq. (15), including the settling velocity function, the sludge removal source term, Eq. (16), and the turbulent dispersion coefficient, $\mu_{\mathrm{t}}/\sigma_{\mathrm{s}}$, to the CFD model as a user-defined scalar equation in Fluent using UDFs.

## 3. Closure models for sludge properties

### 3.1. Sludge rheology

We have used a rotational viscometer to carry out on-site rheology experiments. These experiments, in which we have varied the sludge concentration (2.8–8.4 g l$^{-1}$) and the temperature (10, 15, and 20 °C), have shown that the non-Newtonian flow behaviour of the activated sludge mixture changes qualitatively depending on the shear rate employed in the experiment. At low shear rates of up to 50 s$^{-1}$ (up to 100 s$^{-1}$ at concentrations greater than 5 g l$^{-1}$), the sludge rheology is well described using the Casson law for pseudo-plastic flow behaviour. The sludge displays Bingham plastic flow behaviour at shear rates exceeding 50 s$^{-1}$ (exceeding 100 s$^{-1}$ at concentrations greater than 5 g l$^{-1}$). The rheology experiments were conducted over 3 consecutive days in April 2005. Although not to the same extent, the experiments were repeated on 1 day and for one temperature in July of the same year. The experiments were repeated to verify whether the sludge flow behaviour is different at times of increased treatment plant loadings. These repeated measurements have shown that the flow behaviour had not changed. We have given a detailed account of this experimental study on the non-Newtonian flow behaviour of activated sludge elsewhere [12].

The flow in secondary clarifiers exerts low shear rates on the activated sludge mixture. The shear rates are largest in the inlet region, where the stream of activated sludge enters the clarifier, reaching values that are on the order of 10 s$^{-1}$. Outside this region, the flow is rather stagnant, and the shear rates are well below 1 s$^{-1}$ [6]. Thus, relating the shear rates that prevail in the clarifier to the shear rates applied in the rheology experiments, the Casson rheology model for pseudo-plastic flow behaviour is used in our CFD model.

The Casson equation for the sludge viscosity, $\mu$, may be given as

$$\mu = \left(\frac{K_1}{\dot{\gamma}^{1/2}} + K_2\right)^2, \tag{17}$$

where $\dot{\gamma}$ is the shear rate, $K_1$ the Casson yield stress parameter, and $K_2$ is the Casson viscosity parameter [17]. Our rheology experiments have shown that $K_1$ depends quadratically on the concentration:

$$K_1 = AX^2 + BX. \tag{18}$$

In our rheology analysis, the viscosity parameter, $K_2$, does not show a clear dependence on $X$ and appears to be independent of the sludge concentration over the range of concentrations studied. Neglecting the yield stress parameter, $K_1$, Dollet found that $K_2$ does not depend on the sludge concentration, and he gave a mean value of 0.032 kg$^{1/2}$ m$^{-1/2}$ s$^{-1/2}$ for the Casson viscosity parameter [18]. Both Dollet's observation on the concentration dependence of $K_2$ and his mean value for $K_2$ agree well with the results of our study (Table 1).

We have thus assumed that $K_2$ is independent of the concentration for $X \geq X^* = 2\,\mathrm{kg\,m^{-3}}$ and equal to the mean value, $\bar{K}_2$. For the water viscosity value, $\mu_{\mathrm{w}}$, to emerge correctly as $X \to 0$, $K_2$ is assumed to depend linearly on the concentration on the interval $0 \leq X < X^*$.

Thus, for $X \geq X^*$:

$$K_2 = \bar{K}_2, \tag{19}$$

Table 1
Viscosity parameters in Eqs. (18)–(20) for varying temperatures, $T$

| $T$ (°C) | $A$ (m$^{11/2}$ kg$^{-3/2}$ s$^{-1}$) | $B$ (m$^{5/2}$ kg$^{-1/2}$ s$^{-1}$) | $\bar{K}_2$ (kg$^{1/2}$ m$^{-1/2}$ s$^{-1/2}$) | $\mu_{\mathrm{w}}^{1/2}$ (kg$^{1/2}$ m$^{-1/2}$ s$^{-1/2}$) |
|---|---|---|---|---|
| 10 | 0.00307 | 0.0187 | 0.0463 | 0.0362 |
| 15 | 0.00281 | 0.0176 | 0.0445 | 0.0341 |
| 20 | 0.00319 | 0.0146 | 0.0436 | 0.0361 |

The temperature in the clarifier was 15 °C in March and April, and 20 °C in July.

and for $0 \leq X < X^*$:

$$K_2 = \mu_w^{1/2} + \frac{(\bar{K}_2 - \mu_w^{1/2})}{X^*} X. \quad (20)$$

The values for the parameters in Eqs. (18)–(20) are given in Table 1 for three different temperatures. Eqs. (17)–(20) are added to the CFD model using a UDF.

In the sludge rheology model employed by Armbruster, the sludge viscosity is composed of three additive terms: (i) the viscosity of water, (ii) a square root dependence on the sludge concentration, and (iii) a Bingham-type yield stress term [7]. The terms in Armbruster's rheology model were calibrated using different rheology measurements, and all three model components were necessary to give good agreement between measured and computed velocity and concentration fields. The Herschel–Bulkley rheology model for pseudo-plastic flow behaviour, which includes a yield stress, was used in De Clercq's CFD simulations [6]. De Clercq has conducted rheology measurements at sludge concentrations of about 15 g l$^{-1}$ to avoid the occurrence of turbulent roll cells in his measurement annulus (Taylor–Couette effect). He then extrapolated his approximation of the sludge flow behaviour into the region of lower sludge concentrations. The Bingham model used by Dahl needed substantial recalibration of the model parameters to improve the CFD prediction of the sludge concentration and the velocity field [13]. A Bingham model was also used by Lakehal et al., but their CFD modelling results were not compared with measurements [5].

### 3.2. Sludge density

The density of the sludge mixture, $\rho$, depends on the sludge concentration, $X$. This dependence is usually taken to be a linear function, given by

$$\rho = \rho_w + \left(\frac{\rho_p}{\rho_w} - 1\right) X, \quad (21)$$

where $\rho_w = 998.2\,\text{kg m}^{-3}$ is the density of water, and $\rho_p$ is the density of the dry sludge [3,5,13].

Dahl [13] and Nopens [19] have measured the sludge density as a function of the sludge concentration using pycnometry. Their measurements have confirmed the linear dependence of $\rho$ on $X$, and they have found values for the dry sludge density from a fit of Eq. (21) to their measured data. In the CFD model, we rely on their measurements and use a value of $\rho_p = 1600\,\text{kg m}^{-3}$ for the dry sludge density.

Eq. (21) is used in the CFD model to express the dependence of the sludge density on the sludge concentration in the buoyancy term in Eq. (2), and it is used in Eq. (11) to describe the generation of turbulence kinetic energy due to buoyancy.

### 3.3. Sludge sedimentation

We have conducted batch settling experiments using Applitek's Settlometer [20–22]. This automated device uses a scanner system to detect the height of the sludge blanket during the batch settling experiments, which take place in a column that has a height of 70 cm and a diameter of 14 cm, and that is equipped with a slowly rotating stirrer. We have carried out daily settling experiments at varying initial sludge concentrations of about 2–8 g l$^{-1}$. The sludge was taken at the outlet of the aeration basin, and the initial sludge concentration during the experiments was varied using decantation and dilution. The settling experiments were carried out parallel to the rheology experiments, and we have used sludge taken from the same sampling for both experiments. A typical set of smoothed batch settling curves is shown in Fig. 3.

From the set of batch settling curves, as shown in Fig. 3, we can deduce the parameters $u_{s0}$ and $r_h$ of the exponential settling velocity function of Vesilind [23]:

$$u_s = \left(\frac{dH}{dt}\right)_{max} = u_{s0} \exp(-r_h X). \quad (22)$$

Table 2 summarises the values for $u_{s0}$ and $r_h$ that were obtained from our batch settling experiments in March/April and in July 2005. The results in Table 2 show that the settling behaviour was relatively constant.

Generally, well-settling sludges have $u_{s0}$ and $r_h$ values of about 13 m h$^{-1}$ and 0.25 m$^3$ kg$^{-1}$, respectively. On the other hand, poorly settling sludges have $u_{s0}$ and $r_h$ values of about 5 m h$^{-1}$ and 0.5 m$^3$ kg$^{-1}$, respectively [3]. The parameter values displayed in Table 2 agree well with these criteria. Taking the ratio $u_{s0}/r_h$, we find values of 52 and 10 kg m$^{-2}$ h$^{-1}$ for well settling and poorly settling sludges, respectively. For the sludges

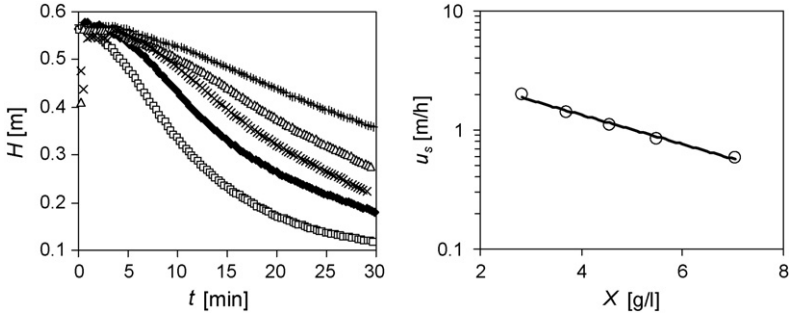


Fig. 3. Typical set of batch settling curves (left) showing the height of the sludge blanket in the settling column, $H$, as a function of the settling time, $t$. The curves were measured on 13 April 2005 and are for sludge concentrations of 2.82 g l$^{-1}$ (□), 3.71 g l$^{-1}$ (♦), 4.56 g l$^{-1}$ (×), 5.48 g l$^{-1}$ (△), and 7.04 g l$^{-1}$ (+). The settling velocity, $u_s = (dH/dt)_{max} = u_s(X)$, is deduced from the batch settling curves (right).

Table 2
Parameters of the Vesilind function, Eq. (22)

| Date | $u_{s0}$ (m h$^{-1}$) | $r_h$ (m$^3$ kg$^{-1}$) |
|---|---|---|
| 21 March 2005 | 5.0175 | 0.3485 |
| 23 March 2005 | 3.9326 | 0.3436 |
| 29 March 2005 | 5.0581 | 0.2723 |
| 30 March 2005 | 4.6398 | 0.2424 |
| 31 March 2005 | 4.3748 | 0.2501 |
| 01 April 2005 | 4.1813 | 0.2495 |
| 11 April 2005 | 5.4402 | 0.3350 |
| 12 April 2005 | 4.0096 | 0.2679 |
| 13 April 2005 | 4.1866 | 0.2844 |
| 14 April 2005 | 4.3210 | 0.2872 |
| 04 July 2005 | 3.0609 | 0.2436 |
| 11 July 2005 | 3.2100 | 0.2247 |
| 19 July 2005 | 4.1338 | 0.3059 |
| 20 July 2005 | 3.5063 | 0.2578 |

studied in the present work, we obtain an average value of about 20 kg m$^{-2}$ h$^{-1}$ for this ratio, which is in the intermediate range.

In addition to $u_{s0}$ and $r_h$, we have measured the stirred sludge volume index ($SSVI_{3.5}$) using Applitek's Settlometer. The $SSVI_{3.5}$ values were found to be in the range 70–105 ml g$^{-1}$, and they were by a factor 0.64 smaller than the values for the diluted sludge volume index (DSVI), which were measured by the plant operator. This value agrees well with the factor of 0.67 given by Ekama et al. [3].

We have correlated the Vesilind parameters, $u_{s0}$ and $r_h$, with the $SSVI_{3.5}$ values using the general correlation equations [3]:

$$u_{s0} = \alpha \exp(-\beta \times SSVI_{3.5}) \quad (23)$$

and

$$r_h = \delta \times SSVI_{3.5} + \gamma. \quad (24)$$

We have found values of 5.5728 m h$^{-1}$ and 0.0034 g ml$^{-1}$ for $\alpha$ and $\beta$, respectively. The correlation for $u_{s0}$ shows that this parameter of the Vesilind function is practically independent of the $SSVI_{3.5}$, since $\beta \approx 0$. This observation agrees well with the results of Daigger's sludge sedimentation study [24], who set $\beta = 0$ and hence $u_{s0} = \alpha$. Daigger found a value of $\alpha = 7.973$ m h$^{-1}$ for the first parameter in Eq. (23), which agrees well with our value for $\alpha$. Similarly, Daigger's values for the parameters in Eq. (24), $\delta = 0.00405$ l ml$^{-1}$ and $\gamma = 0.0538$ l g$^{-1}$, show good agreement with our values ($\delta = 0.0026$ l ml$^{-1}$ and $\gamma = 0.0628$ l g$^{-1}$). In Eq. (23), $u_{s0}$ is in units of m h$^{-1}$, and $r_h$ in Eq. (24) is in units of l g$^{-1}$. The $SSVI_{3.5}$ values are in units of ml g$^{-1}$ in both equations.

In our CFD model, we have used the values for $u_{s0}$ and $r_h$ that were directly measured and that are given in Table 2. The settling velocity is expressed using the double-exponential function of Takács et al. [25], an extension of the Vesilind formula that contains two additional parameters and that is given by

$$u_s = u_{s0} \exp[-r_h(X - X_{ns})] - u_{s0} \exp[-r_p(X - X_{ns})]. \quad (25)$$

The parameter $r_p$ characterises the settling behaviour at low concentrations, and $X_{ns}$ is the concentration of non-settleable solids in the effluent of the clarifier. We have measured $X_{ns}$ by means of decantation, which gave a value of $5.2 \times 10^{-3}$ kg m$^{-3}$. The value for $r_p$ is generally one order of magnitude larger than that of $r_h$, and we thus take $r_p = 10 \times r_h$ [3]. Fig. 4 shows the fit of Eq. (25) to the experimental data displayed in Fig. 3.

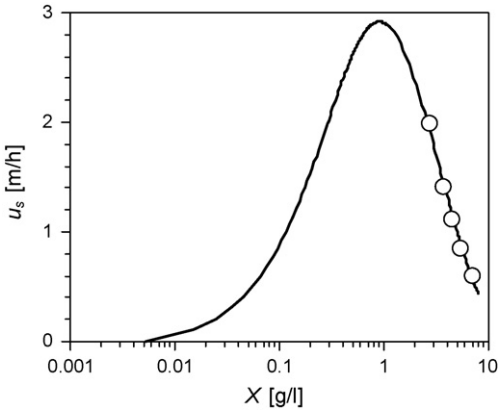


Fig. 4. Fit of the double-exponential settling velocity function, Eq. (25), to the experimental settling velocity data (symbols) that were measured on 13 April 2005. The parameter values are $u_{s0} = 4.1866$ m h$^{-1}$, $r_h = 0.2844$ m$^3$ kg$^{-1}$, $r_p = 10 \times r_h$, and $X_{ns} = 5.2 \times 10^{-3}$ kg m$^{-3}$.

To prove the validity of Eq. (25) over the entire concentration range, measured settling velocities at concentrations below 2 g l$^{-1}$ would have been necessary. We have not been able to obtain reliably measured data in this range of concentrations using our measurement device. However, the settling velocity measurements of Dupont and Dahl confirm the behaviour at low sludge concentrations as described by Eq. (25) [26]. Their measurements show that $u_s$ passes through a maximum at $X \sim 1$ g l$^{-1}$ and that $u_s$ decreases with decreasing sludge concentration at $X < 1$ g l$^{-1}$.

In their original work, Takács et al. [25] expressed the concentration of non-settleable solids in the effluent, $X_{ns}$, using a non-settleable fraction, $f_{ns}$, of the clarifier inlet concentration, $X_{in}$. Takács et al. employed $f_{ns} = 0.00123$, 0.00228, and 0.00259 to distinguish between the cases of low, medium, and high clarifier loadings, respectively. Assuming concentrations of $X_{in} = 3$ and 5 g l$^{-1}$ for the cases of low and high clarifier loading, we find values of $X_{ns} = 3.7$ and 13.0 mg l$^{-1}$, respectively. The value for $X_{ns}$ used in our CFD model corresponds thus well to the criteria of Takács et al. for low to medium clarifier loading. At concentrations ranging from about 0.2–2.0 g l$^{-1}$, and stating that the sludge flocs reach their maximum size in this concentration region, the authors have taken the settling velocity to be independent of the concentration. Imposing this constraint on the settling velocity, Takács and co-workers obtained good agreement between their one-dimensional modelling results and concentration profile measurements.

The double-exponential settling velocity function for $u_s = u_s(X)$ has been used widely in CFD models of secondary clarifiers [5,6,15,16,27–29]. From a practical point of view, the Takács formula for $u_s$ provides an easy-to-use function to characterise the sedimentation of sludge over the entire concentration range. However, the description of the settling velocity at low concentrations in the Takács formula represents a coarse approximation of the individually settling sludge particles. Further, the

compression of sludge at high concentrations is not accounted for in this settling velocity formula.

Other approaches to describe the settling velocity of activated sludge were used in connection with flocculation models. For example, Lyn et al. have assigned individual settling velocity values that came from measurements to each class of particles in their CFD sludge flocculation model [30]. In the two-component CFD model of Mazzolani et al., Eq. (25) was used to describe the settling velocity of larger sludge flocs, and an equation that relates the settling velocity of smaller sludge particles to their diameter was employed to express the settling velocity of this second component [31]. Some researchers have applied Eq. (25) to primary clarifiers, which precede the activated sludge aeration basin [32,33].

The double-exponential settling velocity function was also employed by Armbruster in his clarifier CFD model, but only up to a critical sludge concentration value [7]. Above this critical concentration value, Armbruster used a settling velocity function that considers the compression of sludge. During compression settling (or thickening), the sludge flocs are in mutual contact and become part of a sludge matrix that is compressed by the pressure of the upper sludge layers. The water that is contained in this matrix of sludge is released through channels in the matrix. Gravity-thickening of sludge may thus be understood as the flow (or filtration) of liquid through a deforming saturated flocculent medium [34].

Following an approach proposed by Vaccari and Uchrin [35], Armbruster included a dependence on the spatial concentration gradient in his settling velocity function. In this approach, an increase in the concentration gradient reduces the settling velocity, which in turn reduces the concentration in the thickening layer and therefore the concentration gradient. Thus, sludge concentration and settling velocity are coupled through the concentration gradient.

## 4. Computational domain and sludge removal zone

The clarifier has a depth of $H_{\text{clarifier}} = 3$ m everywhere and a diameter of $D = 33$ m (Fig. 5). Settled sludge is removed from the bottom region of the clarifier by means of suction-lift through an array of vertical suction pipes (Fig. 2). The suction-lift sludge withdrawal mechanism disturbs the otherwise axisymmetric geometry of the clarifier. To reduce computational efforts, we have abstracted the sludge withdrawal mechanism with a disk-like sludge removal zone in the near-bottom region of the clarifier in our axisymmetric CFD model. In the CFD model, sludge is thus removed everywhere in the near-bottom region of the clarifier. The computational domain of the clarifier is shown in Fig. 5, where the disk-like sludge removal zone in the near-bottom region of the clarifier is indicated by the hatched area. In total, about 44,000 regular mesh elements are used for the discretisation of the computational domain. Each mesh element has a characteristic length of about 3 cm.

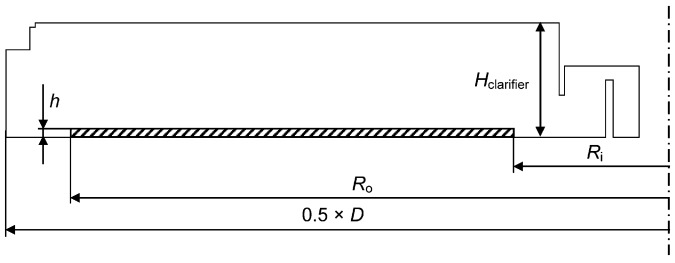


Fig. 5. Computational domain and sludge removal zone of the axisymmetric clarifier model. The centre line of the clarifier is indicated by the dash-dotted line, and the hatched area at the clarifier bottom represents the sludge removal zone in the model (not to scale). $R_i = 3.7$ m, $R_o = 14.7$ m, $h = 0.15$ m, $H_{\text{clarifier}} = 3$ m, and $D = 33$ m.

The volume of the sludge removal zone, $V_{\text{rec}}$, can be calculated using

$$V_{\text{rec}} = \pi(R_o^2 - R_i^2)h. \tag{26}$$

With an inner radius of $R_i = 3.7$ m, an outer radius of $R_o = 14.7$ m, and a height of $h = 0.15$ m from the clarifier bottom, the volume of the sludge removal zone is $V_{\text{rec}} = 2.86\,\text{m}^3$. The height of the sludge removal zone, $h$, corresponds to the distance between the lower end of the suction pipes and the clarifier bottom. The distance $R_o$–$R_i = 11.0$ m corresponds to the length of the array of suction pipes underneath the bridge.

In the physical situation, the settled sludge is withdrawn from the clarifier through the suction pipes, which have an opening area that is smaller than the area of the sludge removal zone used in the CFD model. The local fluid velocities in the region of sludge withdrawal are thus greater than the CFD model can admit, if the same amount of sludge is to be withdrawn. In the region of sludge removal, the CFD model may thus predict lower levels of mixing and turbulence when compared to the values that occur locally in the real settling tank. Another deficiency of our axisymmetric CFD model is the fact that the directionality of the suction pipes is not accounted for. A three-dimensional CFD model would have been necessary to give a better representation of the flow pattern around the complicated sludge removal mechanism of the clarifier. However, such a model would come at much higher computational costs than the simplified model presented in this paper.

## 5. Numerical solution procedure

The general-purpose CFD solver Fluent uses the finite-volume method to discretise the set of governing field equations. A second-order upwind scheme was used for the discretisation in space, and a second-order implicit scheme for the discretisation in time. Employing a segregated solving algorithm in combination with Fluent's SIMPLE algorithm for the pressure-velocity coupling, we have computed the steady-state conditions using a time-marching procedure to facilitate the convergence of the computations. Fluent's pressure staggering option (PRESTO!) is used to interpolate the pressure values between neighbouring elements.

To ensure that the computations have reached steady-state conditions, we have performed the mass balances around the clarifier for both the total fluxes and the sludge fluxes. Another convergence criterion was the local sludge distribution in the clarifier. Using three vertical concentration profiles at varying

radial distances from the clarifier centre, we have compared the profiles computed at time $t$ with those at time $t+\Delta t$, where $\Delta t = 10{,}000$ s. Depending on the values chosen for the initialisation of the flow variables, convergence was attained after about 300,000 s.

## 6. Boundary conditions

### 6.1. Clarifier inlet

At the clarifier inlet, we apply the inlet concentration, $X_{in}$, which is obtained from measurements and which equals the concentration at the outlet of the aeration basin, and the inlet velocity components, $u_{in}$ and $v_{in}$. The radial component of the inlet velocity is set to zero, $v_{in} = 0$. The axial component of the inlet velocity is determined by the flow rate and the cross-sectional area of the inlet annulus, hence

$$u_{in} = \frac{Q_{in}}{\pi(R_{a,o}^2 - R_{a,i}^2)}, \tag{27}$$

where $R_{a,o} = 1.0$ m and $R_{a,i} = 0.3$ m are the outer and the inner radius of the inlet annulus, respectively, and $Q_{in}$ is the flow rate at the clarifier inlet. The latter is obtained from the measured flow rates of the recycle stream and in the effluent outlet canal, and a mass flow balance around the clarifier.

We have installed a Miltronics XPS10 ultrasonic flow metering sonde above the open effluent outlet channel of the clarifier to measure the height of water in the channel. These height measurements, together with the known geometry of the channel, were then used to calculate the effluent flow rate using a weir formula. In addition to the effluent flow rate data, we have used the data of the flow rate in the recirculation stream, which is continuously measured by the process control system of the wastewater treatment plant. Balancing the flow rates around the clarifier gave the flow rate at the inlet of the clarifier.

The flow rates that were measured on 7 July 2005 are shown in Fig. 6. The concentration profile measurements on that day were carried out from about 9:30 to 10:30 in the morning (see Fig. 8). The flow rates show substantial variations over time. However, our concentration profile measurements—which were measured over time and at varying locations in the clarifier, due to the rotation of the clarifier bridge—have shown that the effect of these changing flow rates on the sludge blanket height and the distribution of sludge within the sludge blanket are negligible. The flow rate value for $Q_{in}$, which is used in Eq. (27) to calculate $u_{in}$, was thus averaged using flow measurement data that were recorded during (∼1 h) and before (∼3 h) the concentration profile measurements.

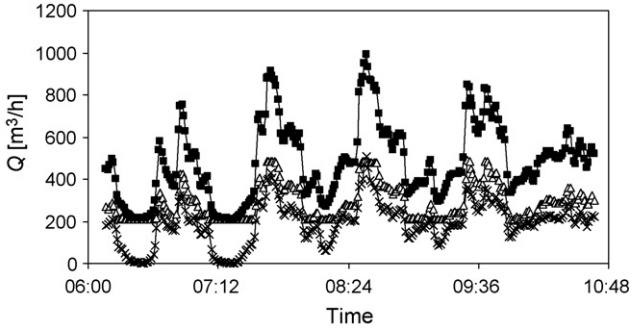


Fig. 6. Flow rates, $Q$, measured at the effluent outlet (×) and in the recycle stream (△). The flow rate at the clarifier inlet (■) was obtained from a flow balance around the clarifier. The data were measured in the morning of 7 July 2005.

We note that when balancing the flow rates around the clarifier, we have made the supposition that any change in flow rate at the inlet of the clarifier is instantaneously measurable at the effluent outlet, so that damping effects of the (large) clarifier volume are not considered. This assumption implies that the up and down movement of the surface, which is small compared to the depth of the clarifier, is neglected.

The turbulence kinetic energy at the inlet, $k_{in}$, is calculated using

$$k_{in} = 1.5 \times (I_u u_{in})^2, \tag{28}$$

where $I_u = 0.025$ is the turbulence intensity [5]. Its dissipation rate at the inlet, $\varepsilon_{in}$, is obtained from

$$\varepsilon_{in} = \frac{C_\mu^{3/4} k_{in}^{3/2}}{\kappa L_u}, \tag{29}$$

in which $\kappa = 0.4$ is the von Kármán constant. The turbulence length scale, $L_u = 0.5 \times R_{baffle}$, where $R_{baffle}$ is the radius of the baffle skirt in the inlet region of the clarifier, is calculated using the recommendations of Lakehal et al. [5].

### 6.2. Free surface

The vertical movement of the free surface of the clarifier is assumed to be negligibly small. This assumption simplifies the computation greatly, as it helps to keep the computational efforts to a minimum. The vertical (axial) velocity component is thus set to zero at the surface, $u = 0$, and the horizontal (radial) velocity component, $v$, is computed assuming full slip, that is, the surface is treated as a stress-free entity. Furthermore, the gradients of all scalar variables ($X$, $k$, and $\varepsilon$) normal to the surface are set to zero, and the same condition applies to the gradient of the radial velocity in the direction normal to the surface, that is, $\partial v/\partial z = 0$.

### 6.3. Effluent outlet

At the effluent outlet boundary, the values of the variables are extrapolated from computed near-outlet values. This extrapolation sets the stream-wise gradients to zero.

### 6.4. Solid walls

The no-slip condition must be obeyed at all solid boundaries, that is, $u, v = 0$ at all clarifier walls. The boundary condition on the concentration is that the gradients perpendicular to all solid walls is set to zero, so that the solid walls are made impenetrable for the scalar species. We also apply logarithmic wall functions to model the turbulent flow in the near-wall region of the clarifier. Using this approach—which applies to the velocities,

the concentration, and the turbulent variables—the viscosity-affected near-wall region is not resolved by the mesh. Instead, a collection of semi-empirical equations is used to link the solution variables in the near-wall cells and the corresponding quantities on the wall.

## 7. Results and discussion

### 7.1. Local sludge distribution in the clarifier

The local sludge distribution in the Clarifier was measured using a Solitax-ts light scattering sonde. The sonde was connected to an aluminium tube of 4.5 m in length that allowed for measuring the sludge concentration down to the bottom of the clarifier. A custom-built support was used to attach the aluminium tube to the clarifier bridge and to easily change both the vertical and the horizontal position of the sonde. The custom-built support enabled us to conduct our profile measurements at a perpendicular distance of 0.5 m from the clarifier bridge at its advancing side. Starting at the bottom of the clarifier, we have taken concentration value readings every 5–10 cm. At least five readings were taken at each vertical position, and the average value of these readings was calculated. We have measured several vertical concentration profiles, usually 3–5, at varying radial distances from the centre of the clarifier along the slowly rotating bridge. Measuring a complete set of concentration profiles took around 50 min, which corresponds roughly to the time required for the clarifier bridge (and therefore for the sludge removal mechanism at the bottom of the clarifier) to circumference the clarifier once. We have used the sludge concentration profile measurements to validate the predictions of our CFD model.

Figs. 7 and 8 show two sets of vertical concentration profiles that were measured in March and July, respectively. In the summer months, the loading of the treatment plant is increased, and more sludge is stored in the clarifier. The concentration profiles show that the sludge blanket height—which we define as the vertical distance from the clarifier bottom to the point at which the sludge concentration falls below 1 g $l^{-1}$—has a value of 40–50 cm in March, and 60–70 cm in July, depending on the radial distance from the centre of the clarifier. The sludge blanket is more elevated at shorter distances from the clarifier centre in both sets of concentration profiles. The measured data show further that the sludge concentration at the clarifier bottom is higher in July, reaching concentration values that exceed 10 g $l^{-1}$. At greater distances from the clarifier centre, the July data show that highly concentrated sludge has accumulated in the bottom region. This accumulation of sludge is presumably caused by the slowly rotating sludge collection system at the clarifier bottom, which compresses the settled sludge and pushes it in the direction of movement of the bridge. The bottom concentration is lower in the close vicinity of the inlet region, where the convective motion of the incoming stream of sludge dilutes and disturbs the sludge that has settled in that region. In March, the bottom concentration was well below 10 g $l^{-1}$, and we did not observe the accumulation of highly concentrated sludge in the near-bottom region that occurred in July.

The comparison between computed and measured concentration profiles shows that the CFD model is well capable of predicting the local sludge distribution in the clarifier. For both

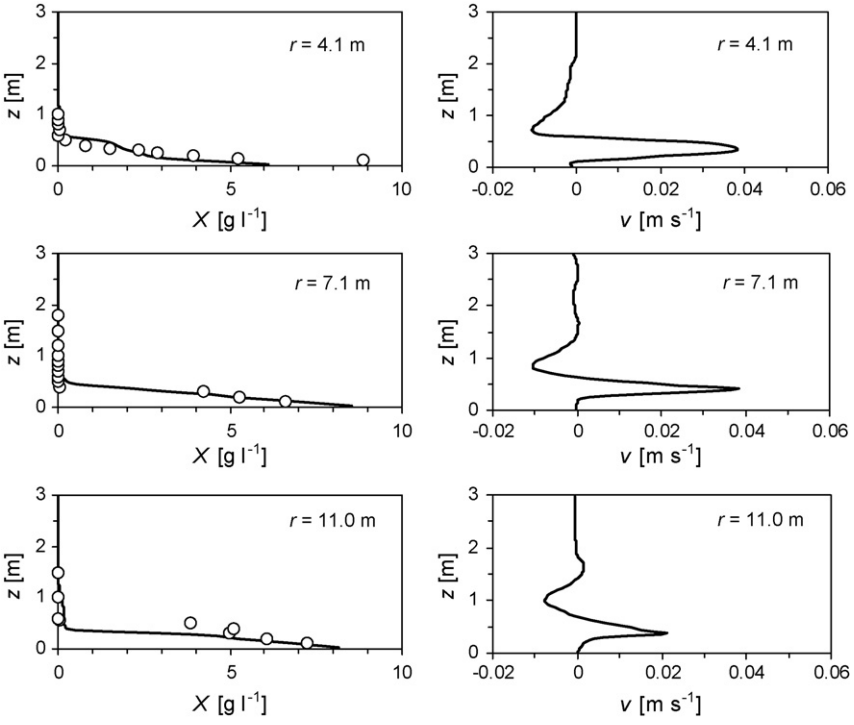


Fig. 7. Activated sludge concentration, $X$, and radial velocity, $v$, profiles in the clarifier between the surface ($z = H_{clarifier} = 3$ m) and the bottom of the clarifier basin ($z = 0$). The data are for 31 March 2005 ($X_{in} = 3.91$ g $l^{-1}$, $u_{in} = 0.049$ m $s^{-1}$, $q_{rec} = 75.7$ kg $s^{-1}$) and are for varying radial distances, $r$, from the clarifier centre. The CFD predictions of the concentration profiles are compared with measurements (symbols).

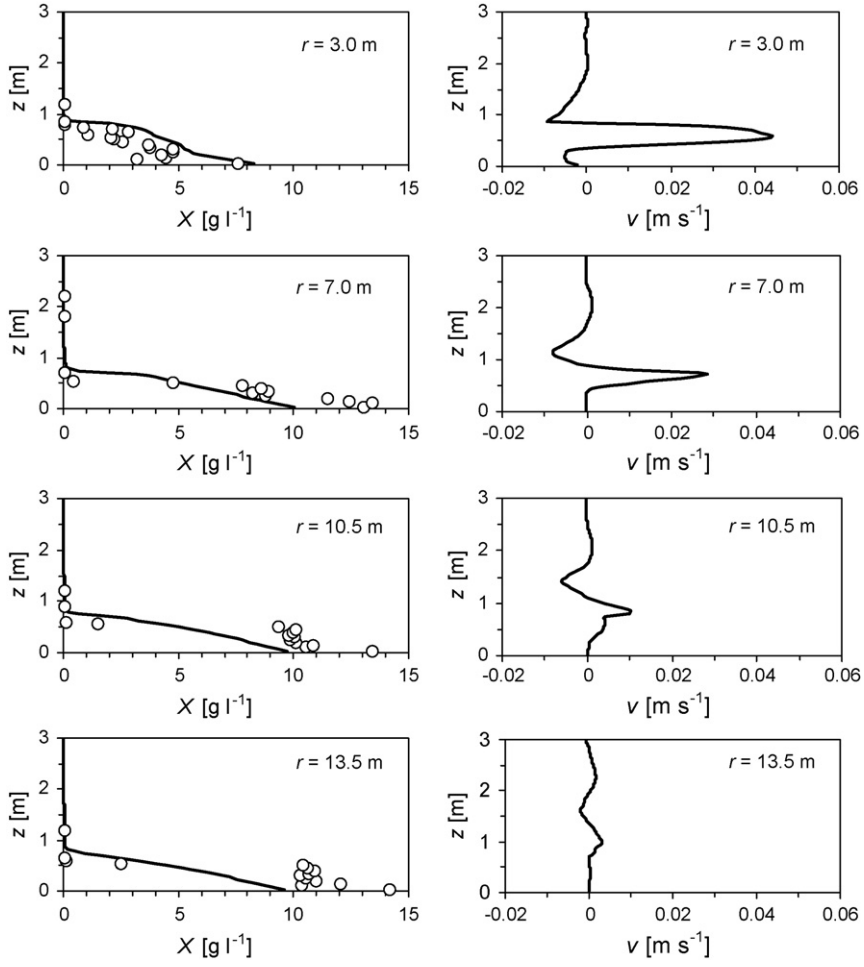


Fig. 8. Activated sludge concentration, $X$, and radial velocity, $v$, profiles in the clarifier between the surface ($z = H_{\text{clarifier}} = 3$ m) and the bottom of the clarifier basin ($z = 0$). The data are for 7 July 2005 ($X_{\text{in}} = 4.93\ \text{g l}^{-1}$, $u_{\text{in}} = 0.065\ \text{m s}^{-1}$, $q_{\text{rec}} = 100.4\ \text{kg s}^{-1}$) and are for varying radial distances, $r$, from the clarifier centre. The CFD predictions of the concentration profiles are compared with measurements (symbols).

the March and the July data, the CFD model reproduces the sludge distribution in the region close to the inlet well. In the case of the July data, the CFD model slightly over-predicts the height of the sludge blanket away from the inlet region. This over-prediction may be caused by unequal sludge withdrawal through the individual suction pipes or by the dynamically varying flow rates at the clarifier inlet and in the sludge recycle stream during the measurements. In the CFD model, the same amount of sludge is removed in each element in the sludge removal zone. We do not account for the individual flow rates in each of the suction pipes, which are likely to differ somewhat from each other. Instead, we take the total amount of sludge that is withdrawn from the clarifier bottom, $q_{\text{rec}}$, and relate this amount to the total volume of the sludge removal zone in the CFD model, $V_{\text{rec}}$. Additional measurements of the sludge flow rates in each suction pipe may help to improve the prediction of the sludge blanket height by the CFD computations further.

Although the prediction of the bottom concentration values agrees well with the values measured in March, the CFD model is not capable of predicting the much higher bottom concentrations that were measured in July, presumably as a consequence of the three-dimensional effects of the sludge collection mechanism, which we do not consider in the two-dimensional CFD model. However, the average concentration value in the sludge removal zone of the CFD model ($9.04\ \text{g l}^{-1}$) corresponds very well to the concentration value that was measured in the recycle stream ($9.71\ \text{g l}^{-1}$). The computed effluent concentration values for the March and July data are 10.7 and $12.9\ \text{mg l}^{-1}$, respectively, and they agree well with the averaged measured effluent concentration of $11\ \text{mg l}^{-1}$.

### 7.2. Velocity field and density current in the clarifier

The computed vertical velocity profiles in Figs. 7 and 8 show the radial velocity component, $v$, as a function of the axial clarifier coordinate, $z$, and for varying radial distances from the clarifier centre, $r$. We have plotted the radial velocity component to illustrate the density current along the upper limit of the sludge blanket.

The profiles show that the flow is very calm in the clear water region of the clarifier, above the sludge blanket. Significant flow velocities are encountered a short vertical distance above and below the upper limit of the sludge blanket. The velocities are largest in the inlet region and become smaller with increasing

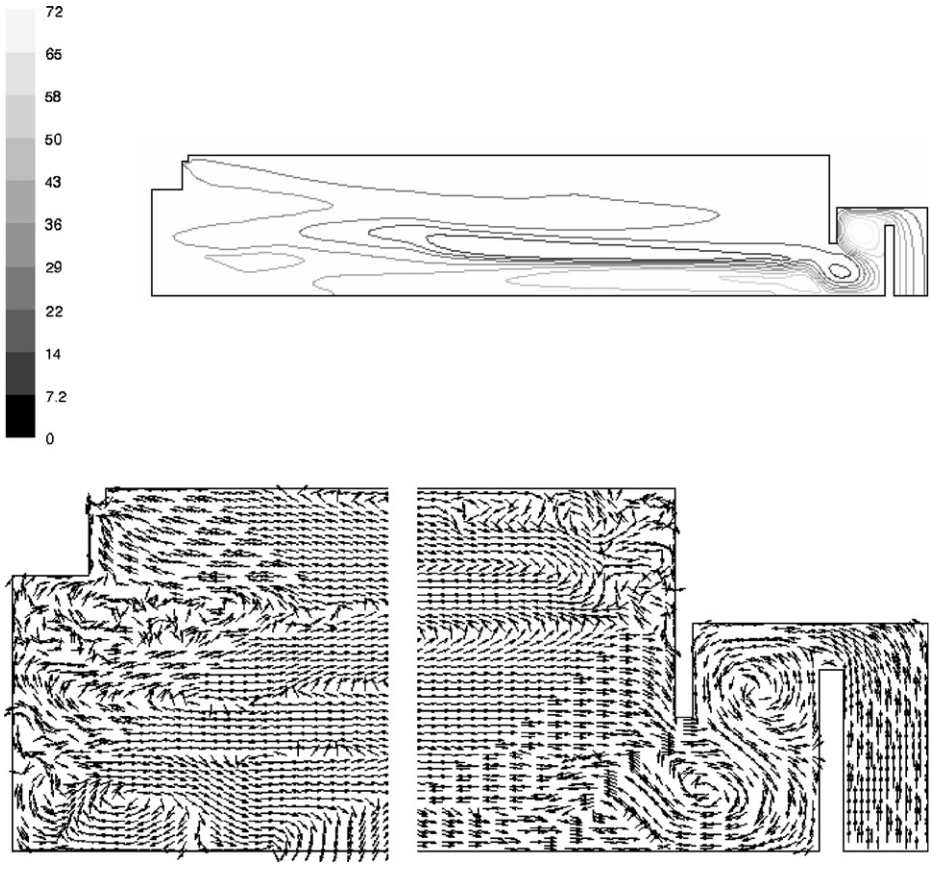


Fig. 9. Stream functions (top), in units of kg $s^{-1}$, and velocity vectors in the region underneath the effluent outlet (bottom left) and in the inlet region (bottom right). The computations are for 7 July 2005 ($X_{in} = 4.93\ g\ l^{-1}$, $u_{in} = 0.065\ m\ s^{-1}$, $q_{rec} = 100.4\ kg\ s^{-1}$). Note that only every other vector is shown in the velocity vector plots in both the axial and the radial direction and that a uniform length scale has been assigned to each vector shown in the plots.

radial distance from the centre of the clarifier. In addition to the convective motion of the incoming sludge mixture, the density difference between the sludge and the clear water above the sludge blanket transports the sludge into the clarifier along the upper limit of the sludge blanket. This buoyancy force is weakened with increasing radial distance from the inlet region by the viscous forces that dominate the flow within the sludge blanket, as shown in the next section of this paper. The strong viscous forces within the sludge blanket are also responsible for the low velocities in that region of the clarifier basin. In a circular clarifier, the velocity is further reduced by the increasing cross-sectional area with increasing distance from the centre. The graphs in Figs. 7 and 8 show that the vertical position of the positive peak velocity coincides with the height of the sludge blanket, where the sludge density gradient is largest.

The velocity profiles in the clarifier show negative velocities above and below the upper limit of the sludge blanket. These negative velocities correspond to zones of flow reversal and recirculation in the clear water region and in the near-bottom region. Fig. 9—which shows the streamlines and the velocity vectors in the regions next to the clarifier inlet and underneath the effluent outlet—illustrates these zones of flow reversal and recirculation. We note that in the plots of the vector field, to improve the visual appearance of the zones of recirculation, we have plotted only every other vector in both the axial and the radial direction. Furthermore, we have assigned a uniform length to each vector, so that the length of each vector does not correspond to its true velocity value.

The velocity profiles shown in Figs. 7 and 8 are typical for both rectangular and circular centre-fed clarifiers. Krebs et al., using glass spheres and a rectangular laboratory-scale sedimentation tank, have performed velocity profile measurements that matched their numerical predictions of the bottom density current very well [14]. Dahl et al. measured velocity profiles in a rectangular pilot sedimentation tank, which had been installed on a wastewater treatment plant and that was fed with activated sludge from the aeration basin [36]. Although their CFD calculations of the density current in the pilot sedimentation tank agreed well with measured velocity profiles, the agreement was less good in the case of full-scale rectangular sedimentation tanks [13].

A radioisotope tracer technique was used by Kim et al. to study the flow in a rectangular full-scale clarifier [37]. An impulse injection of tracer at the outlet of the aeration basin was applied, and the residence time distribution (RTD) of the tracer material was monitored at 20 different points in the clarifier. The authors have further measured the sludge concentration at the inlet and at the effluent outlet of the clarifier. The RTD measurements and the measured effluent concentration were compared with the computed RTD and effluent concentration value of

a two-dimensional numerical model of the turbulent flow and mass transport in the clarifier. The mathematical description of the numerical model that was used by Kim et al. is essentially identical with the CFD model presented in this paper, except for the description of the viscosity, where Kim et al. neglected the molecular viscosity of the activated sludge mixture. The authors have further tested two approaches for the settling velocity function—the double-exponential function used in this paper and a discrete settling velocity function. The latter function, which was also used by Mazzolani et al. to describe the sedimentation of individual sludge particles at low concentrations [31], assumes that the settling velocity is a function of the particle diameter.

The authors obtained good agreement between measured and calculated RTD near the inlet and in the centre of the clarifier. Near the effluent outlet, the agreement was less good, which the authors attribute to the three-dimensional effects of the discharge weir in this region of the clarifier, which is not considered in their two-dimensional model. A second peak in the measured RTD indicated local flow reversal, which was partially confirmed by the computed RTD. Referring to the removal efficiency in the clarifier, the discrete settling model predicts a value of 98.4% for the average solids distribution. Using the mono-disperse (double-exponential) settling model, a lower value of 94.3% is calculated.

The inlet sludge concentration in their study was relatively low, at only $1.3\,g\,l^{-1}$. Relating the removal efficiency that was calculated by Kim and co-workers using the discrete settling model to this inlet concentration, we obtain a value of $20.8\,mg\,l^{-1}$ for the effluent concentration, which is a factor 4.2 larger than the average measured value of $5\,mg\,l^{-1}$. The fact that the discrete settling model gives a better prediction of the effluent concentration than the mono-disperse settling model may be due to the low inlet concentration. In the present paper, inlet concentrations of 3.9 and $4.93\,g\,l^{-1}$ were studied. As we have discussed in Section 7.1, our CFD model gave predictions of the effluent concentration that differed by a factor of 0.97 and 1.17 from the averaged measured value. Furthermore, our CFD model accounts for the complex rheological flow behaviour of the activated sludge mixture. Kim and co-workers neglected the sludge rheology, which, through the coupling between viscosity, sludge concentration, and shear rate, affects the sludge distribution and therefore the effluent concentration.

### 7.3. Shear rate and sludge viscosity in the clarifier

A contour plot of the shear rates in the clarifier is shown in the top of Fig. 10. It shows that the highest shear rates are encountered in the inlet region, where the incoming stream of activated sludge is bound by the walls and baffles in that region, and around the upper limit of the sludge blanket, close to the clarifier inlet. The elevated shear rates around the upper limit of the sludge blanket are caused by the density current, which is strongest in the inlet region of the clarifier. Above the sludge blanket, and for the most part also within the sludge blanket, the shear rates are below $0.1\,s^{-1}$ (blank area in the top contour plot in Fig. 10). De Clercq's CFD computations of the flow and the sludge sedimentation in a secondary clarifier with bottom inclination and sludge removal through the sludge hopper in the bottom centre of the clarifier exhibit similar shear rate distributions [6].

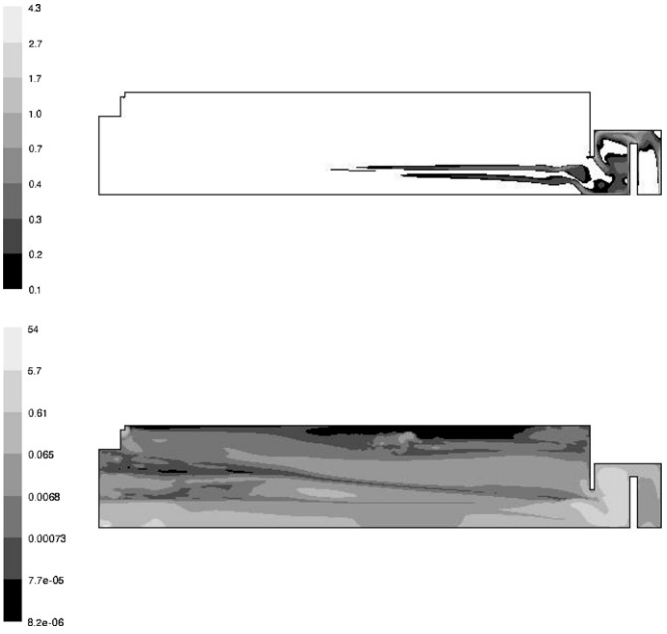


Fig. 10. Shear rates (top), $\dot{\gamma}$, in units of $s^{-1}$, and turbulent viscosity (bottom), $\mu_t$, in units of $kg\,m^{-1}\,s^{-1}$, in the clarifier for 7 July 2005 ($X_{in} = 4.93\,g\,l^{-1}$, $u_{in} = 0.065\,m\,s^{-1}$, $q_{rec} = 100.4\,kg\,s^{-1}$).

From Eq. (17), we see that the sludge viscosity is inversely proportional to the shear rate, that is, $\mu \to \infty$ as $\dot{\gamma} \to 0$. On the other hand, the viscosity decreases with decreasing concentration, so that $\mu \to \mu_w$ as $X \to 0$. The concentration above the sludge blanket is very low, as shown in Figs. 7 and 8. Thus, although the shear rates are very low above the sludge blanket, the viscosity does not exceed values that equal five times the water value, due to the low sludge concentrations in that region (top of Fig. 11). Within the sludge blanket, where the computed sludge concentration reaches values of almost $10\,g\,l^{-1}$ in the near-bottom region, the sludge viscosity takes values that are by several orders of magnitude larger than the water value (bottom of Fig. 11). When comparing the high sludge viscosity values within the sludge blanket with the values of the turbulent viscosity, which are shown in the contour plot in the bottom of Fig. 10, we see that the sludge viscosity dominates the flow within the sludge blanket. Above the sludge blanket the turbulent viscosity contribution may not be neglected, as both the sludge viscosity and the turbulent viscosity are mostly of the same order of magnitude.

Deininger et al. have used a numerical two-phase flow model to compute the flow and the solids distribution in a circular clarifier [38]. Their model does not account for the non-Newtonian flow behaviour of the activated sludge mixture. Instead, the authors have taken the viscosity value of water, that is, $\mu = \mu_w = 10^{-3}\,kg\,m^{-1}\,s^{-1}$. They have compared their model predictions with measurements of both the radial and vertical velocities in the clarifier and the local solids distribution.

A forward flow along the tank bottom towards the outer tank rim and a backward flow in the upper (clear water) region of the

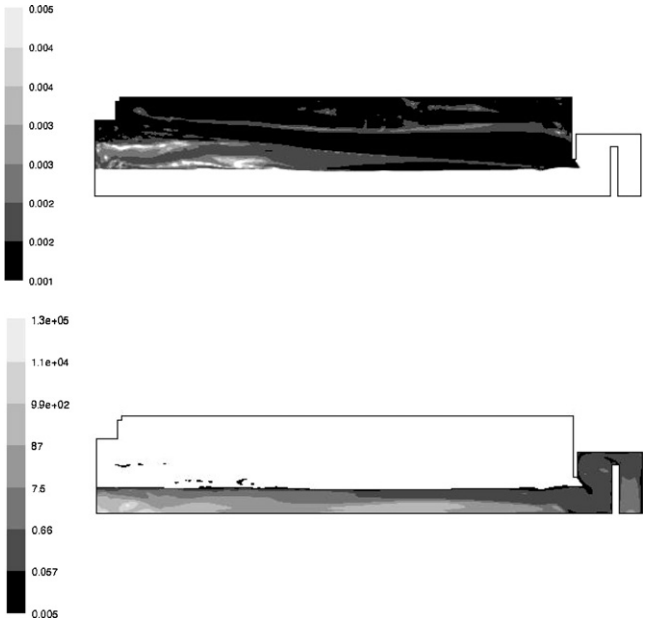


Fig. 11. Sludge viscosity, $\mu$, in units of kg m$^{-1}$ s$^{-1}$, in the clarifier for 7 July 2005 ($X_{in}$ = 4.93 g l$^{-1}$, $u_{in}$ = 0.065 m s$^{-1}$, $q_{rec}$ = 100.4 kg s$^{-1}$). The contour plots show the sludge viscosity above (top) and within (bottom) the sludge blanket.

clarifier towards the centre of the clarifier were shown in both velocity measurements and computations. However, the area of computed forward velocities is larger than the measured area. To obtain better agreement between model prediction and measurements, Deininger et al. have assigned a constant value of $\mu_t = 0.1$ kg m$^{-1}$ s$^{-1}$ to the turbulent viscosity. This value is two orders of magnitude larger than the water value, $\mu_w$. The $k$–$\varepsilon$ turbulence model and the closure model to calculate $\mu_t$ were thus not used. The authors report that this measure reduced the computed area, in which flow reversal occurs, and it improved the agreement between measurements and computations. Similar observations were made in the case of the calculated and measured downward velocities in the clarifier inlet region, which differed by a factor of about 2. Using $\mu_t = 0.1$ kg m$^{-1}$ s$^{-1}$, Deininger and co-workers could predict downward velocities in the inlet region that agree with the measured values.

The concentration field, and in particular the sludge concentration at the bottom of the settling tank, was well predicted by the numerical model. However, from $r = 7$ m to the outer rim at $r = 12$ m, the model predicted virtually no sludge accumulation at the bottom, which disagrees strongly with the concentration measurements. This discrepancy between model prediction and measurements was attributed to sludge conveyance by the bottom scraper, which is not considered in the numerical model. However, it does not seem to be evident that this disagreement between the computed and measured concentration field is caused by the bottom scraper, since it had been kept from moving during the measurements, as stated by the authors.

The observations made by Deininger et al. show that the viscosity plays an important role in predicting both the velocity and the concentration field in the clarifier. Instead of using a different approach to describe the molecular viscosity of the activated sludge mixture, Deininger and co-workers have set the value of the turbulent viscosity to a constant value that is much larger than the viscosity value of water. In the present paper, we have computed the turbulent viscosity using the $k$–$\varepsilon$ turbulence model, and the molecular viscosity of the sludge mixture is described using a non-Newtonian closure model, which is based on our rheology measurements. The agreement between the measured and the computed concentration field that we have obtained shows that the $k$–$\varepsilon$ turbulence model is an adequate means to describe the turbulent viscosity, provided the rheological flow behaviour of the sludge mixture is considered. Similar conclusions can be drawn from the works of Dahl [13], Lakehal et al. [5], De Clercq [6], and Armbruster [7].

## 8. Conclusions

This paper presents a computational fluid dynamics (CFD) model of the flow and the sedimentation of activated sludge in a full-scale flat-bottom clarifier that is equipped with a suction-lift sludge removal system. Negative source terms on all field equations were used to approximate the removal of sludge in the bottom region of the clarifier in the two-dimensional CFD model. The clarifier CFD model, which was developed using the general-purpose CFD solver Fluent, accounts for the turbulent motion in the clarifier and considers buoyancy-driven flow. Our on-site rheology measurements have shown that the activated sludge mixture exhibits pseudo-plastic flow behaviour at shear rates that are comparable to those encountered in the clarifier. The Casson rheology model was used to describe the non-Newtonian flow behaviour of the activated sludge mixture in the CFD model. Using the double-exponential settling velocity function, the sedimentation of activated sludge flocs was incorporated in the axial convection term of the convection–dispersion equation that governs the sludge transport in the clarifier. The parameters of the settling velocity function were obtained from on-site sedimentation measurements.

Measured sludge concentration profiles were compared with CFD predictions of the local sludge distribution in the clarifier. The concentration profiles that were computed by the CFD model agree well with measured profiles for two different treatment plant loadings. The CFD model reproduces the local sludge distribution in the inlet region, where the incoming sludge mixture dilutes and disturbs the sludge that has settled in this part of the clarifier. In the case of the higher inlet concentration, the CFD model slightly over-estimates the height of the sludge blanket. This over-estimation may be due to the dynamically changing flow rates at the clarifier inlet and in the sludge recycle stream during the measurements. Unequal sludge withdrawal through the individual suction pipes of the sludge-removal mechanism may be another explanation for this over-estimation. For the same set of experimental data, the CFD model is not capable of predicting the high bottom concentrations. These high bottom concentrations are presumably due to the accumulation of compressed sludge at the advancing side of the slowly rotating sludge collection mechanism, which is not accounted for in our two-dimensional CFD model. The CFD model has shown that within the sludge blanket, the flow and the sedimentation of sludge is dominated by the viscous forces, and the effects of the

turbulent viscosity contribution are negligible within the sludge blanket.

We have simplified the representation of the sludge removal mechanism in our CFD model. A correct representation of this complex system requires a three-dimensional model, which would come at significantly increased computational costs. The model presented in the present paper predicts the sludge distribution in the clarifier well, at reasonable computational expenses. In combination with design rules, the CFD model helps the design engineers to calculate different clarifier loading scenarios and to ensure the proper functioning of the secondary clarifier under all loading conditions. The geometry and the inlet and outlet configuration of existing clarifiers may be optimised using the CFD model. The effect of varying sludge properties on the clarifying, thickening, and storage capacities of the clarifier may be studied and assessed.

## Acknowledgements

M. Weiss and B.Gy. Plósz gratefully acknowledge financial support from the European Commission for two industry-host Marie Curie postdoctoral research fellowships. The authors thank Dr. Cyril Printemps-Vacquier and the members of staff at the wastewater treatment plant for their support and excellent collaboration during the on-site measurement campaigns.

## References

[1] P.N. Cheremisinoff, Handbook of Water and Wastewater Treatment Technology, Marcel Dekker Inc., New York, 1995.
[2] U. Jeppson, Modelling Aspects of Wastewater Treatment Processes, PhD Thesis, Lund Institute of Technology, Sweden, 1996.
[3] G.A. Ekama, J.L. Barnard, F.W. Günthert, P. Krebs, J.A. McCorquodale, D.S. Parker, E.J. Wahlberg, Secondary Settling Tanks: Theory, Modelling, Design and Operation, IAWQ, London, 1997.
[4] S.D. Lin, Water and Wastewater Calculations Manual, McGraw-Hill, New York, 2001.
[5] D. Lakehal, P. Krebs, J. Krijgsman, W. Rodi, Computing shear flow and sludge blanket in secondary clarifiers, J. Hydr. Eng. (1999) 253–262.
[6] B. De Clercq, Computational Fluid Dynamics of Settling Tanks: Development of Experiments and Rheological, Settling, and Scraper Submodels, PhD Thesis, University of Gent, Belgium, 2003.
[7] M. Armbruster, Untersuchung der möglichen Leistungssteigerung von Nachklärbecken mit Hilfe numerischer Simulationen, PhD Thesis, University of Karlsruhe, Germany, 2004.
[8] A. Keshtkar, B. Meyssami, G. Abolhamd, H. Ghaforian, M. Khalagi Asadi, Mathematical modeling of non-ideal mixing continuous flow reactors for anaerobic digestion of cattle manure, Bioresource Technol. 87 (2003) 113–124.
[9] M.S. Vesvikar, M. Al-Dahhan, Flow pattern visualization in a mimic anaerobic digester using CFD, Biotech. Bioeng. 89 (2005) 719–732.
[10] K. Essemiani, S. Vermande, S. Marsal, L. Phan, J. Meinhold, Optimisation of WWTP units using CFD—a tool grown for real scale application, in: 2nd IWA Leading-Edge Conference on Water and Wastewater Treatment Technologies, 1–4 June 2004, Prague, Czech Republic.
[11] G.C. Glover, C. Printemps, K. Essemiani, J. Meinhold, Modelling of wastewater treatment plants—how far shall we go with sophisticated modelling tools? Water Sci. Technol. 53 (2006) 79–89.
[12] M. Weiss, B.Gy. Plósz, K. Essemiani, J. Meinhold, Sedimentation of activated sludge in secondary clarifiers, in: 5th World Congress of Particle Technology (WCPT), 23–27 April 2006, Orlando, Florida, US.
[13] C. Dahl, Numerical Modelling of Flow and Settling in Secondary Settling Tanks, PhD Thesis, University of Aalborg, Denmark, 1993.
[14] P. Krebs, A.I. Stamou, J.L. García-Heras, W. Rodi, Influence of inlet and outlet configuration on the flow in secondary clarifiers, Water Sci. Technol. 34 (1996) 1–9.
[15] Z.C. Vitasovic, S. Zhou, J.A. McCorquodale, K. Lingren, Secondary clarifier analysis using data from the clarifier research technical committee protocol, Water Environ. Res. 69 (1997) 999–1007.
[16] T. Matko, N. Fawcett, A. Sharp, T. Stephenson, Recent progress in the numerical modelling of wastwater sedimentation tanks, Trans. IChemE 74 Part B (1996) 245–258.
[17] I. Seyssiecq, J.-H. Ferrasse, N. Rouche, State-of-the-art: rheological characterisation of wastewater treatment sludge, Biochem. Eng. J. 16 (2003) 41–56.
[18] P. Dollet, Application de Mesures Rhéologiques à la Caractérisation de L'Etat de Floculation des Boues Activées, PhD Thesis, University of Limoges, France, 2000.
[19] I. Nopens, Modelling the Activated Sludge Flocculation Process: A Population Balance Approach, PhD Thesis, University of Gent, Belgium, 2005.
[20] P. Vanrolleghem, D. Van der Schueren, G. Krikilion, K. Grijspeerdt, P. Willems, W. Verstraete, On-line quantification of settling properties with in-sensor-experiments in an automated settlometer, Water Sci. Technol. 33 (1996) 37–51.
[21] A. Vanderhasselt, H. Aspegren, P. Vanrolleghem, W. Verstraete, Settling characterisation using on-line sensors at a full-scale wastewater treatment plant, Water SA 25 (1999) 1–6.
[22] A. Vanderhasselt, P.A. Vanrolleghem, Estimation of sludge sedimentation parameters from single batch settling curves, Water Res. 34 (2000) 395–406.
[23] P.A. Vesilind, Design of prototype thickeners from batch settling tests, Water Sewage Works 115 (1968) 302–307.
[24] G.T. Daigger, Development of refined clarifier operating diagrams using an updated settling characteristics database, Water Environ. Res. 67 (1995) 95–100.
[25] I. Takács, G.G. Patry, D. Nolasco, A dynamic model of the clarification-thickening process, Water Res. 25 (1991) 1263–1271.
[26] R. Dupont, C. Dahl, A one-dimensional model for a secondary settling tank including density current and short circuiting, Water Sci. Technol. 31 (1995) 215–224.
[27] S. Zhou, J.A. McCorquodale, Mathematical modelling of a circular clarifier, Can. J. Civ. Eng. 19 (1992) 365–374.
[28] S. Zhou, J.A. McCorquodale, Influence of skirt radius on performance of circular clarifier with density stratification, Int. J. Num. Meth. Fluids 14 (1992) 919–934.
[29] J.A. McCorquodale, S. Zhou, Effects of hydraulic and solids loading on clarifier performance, J. Hydr. Res. 31 (1993) 461–478.
[30] D.A. Lyn, A.I. Stamou, W. Rodi, Density current and shear-induced flocculation in sedimentation tanks, J. Hydr. Eng. 118 (1992) 849–865.
[31] G. Mazzolani, F. Pirozzi, G. D'Antonio, A generalized settling approach in the numerical modeling of sedimentation tanks, Water Sci. Technol. 38 (1998) 95–102.
[32] K. Gernaey, P.A. Vanrolleghem, P. Lessard, Modelling of a reactive primary clarifier, Water Sci. Technol. 43 (2003) 73–81.
[33] G. Sreckovic, E.R. Hall, Computer Simulation of Activated Sludge Clarifiers in the Pulp and Paper Sector, Project Report 2000–2005, Sustainable Forest Management Network, University of Alberta, Canada, 2000.
[34] P. Kos, Gravity thickening of water-treatment-plant sludges, J. AWWA (1977) 272–282.
[35] D.A. Vaccari, C.G. Uchrin, Modeling and simulation of compressive gravity thickening of activated sludge, J. Environ. Sci. Health A24 (1989) 645–674.
[36] C. Dahl, T. Larsen, O. Petersen, Numerical modelling and measurements in a test secondary settling tank, Water Sci. Technol. 30 (1994) 219–228.
[37] H.S. Kim, M.S. Shin, D.S. Jang, S.H. Jung, J.H. Jin, Study of flow characteristics in a secondary clarifier by numerical simulation and radioisotope tracer technique, Appl. Radiation Isotopes 63 (2005) 519–526.
[38] A. Deininger, E. Holthausen, P.A. Wilderer, Velocity and solids distribution in circular secondary clarifiers: full scale measurements and numerical modelling, Water Res. 32 (1998) 2951–2958.